FREQUENCY-DOMAIN REVERSE TIME MIGRATION USING THE L_1-NORM

JEEEUN LEE[1], YOUNGSEO KIM[2] and CHANGSOO SHIN[1]

[1] *Seoul National University, Department of Energy Resources Engineering, 151-744/ 36-2061, College of Engineering, Seoul National Univ., Daehak-dong Gwanak-gu, Seoul, South Korea.*
[2] *Seoul National University, Research Institute of Energy and Resources 151-744/ Building 135, College of Engineering, Seoul National Univ., Daehak-dong Gwanak-gu, Seoul, South Korea. kysgood0@snu.ac.kr*

(Received February 5, 2012; revised version accepted June 1, 2012)

ABSTRACT

Lee, J., Kim, Y. and Shin, C., 2012. Frequency-domain reverse time migration using the L_1-norm. *Journal of Seismic Exploration*, 21: 281-300.

Waveform inversion algorithms generally use the L_2-norm. However, previous work indicates that the L_1-norm objective function can produce better results than the L_2-norm objective function because the L_1-norm is more robust against outliers. Moreover, because field data always contain some outliers, adopting the L_1-norm objective function for waveform inversion would therefore be beneficial. Thus, we consider adopting the L_1-norm for reverse time migration, since the algorithm structure of reverse time migration is identical to that of waveform inversion. Thus, we propose introducing the L_1-norm into frequency domain reverse time migration for 2D acoustic media. To verify the effectiveness of our algorithm, we compare the results with those from the conventional algorithm. First, we apply both algorithms to synthetic data drawn from the Marmousi model. We also apply both algorithms to synthetic data on which we add artificial random outliers. Considering the data without outliers, both algorithms yield similar results regardless of the norm used. However, when we consider the data containing outliers, our algorithm using the L_1-norm yields better results. We then apply the same algorithm to field data obtained from an area in the Gulf of Mexico. As expected from the synthetic test, our algorithm yields superior results. Through these experiments, we conclude that the newly proposed algorithm would be useful for performing reverse time migration on data containing considerable outliers, thus eliminating some preprocessing steps through the use of the L_1-norm.

KEY WORDS: reverse time migration, frequency domain, 2D, L_1-norm, outlier.

0963-0651/12/$5.00

INTRODUCTION

Before migration, processed seismic data are often distorted because of rapid velocity variations, complex structure, steep reflectors, and so on. A migration algorithm is needed to produce a subsurface image under these difficult conditions. Since Whitmore (1983) introduced reverse time migration using the wave equation, reverse time migration technique has been widely studied. Baysal (1983), Loewenthal and Mufti (1983), and other authors studied reverse time migration contemporaneously with Whitmore. However, whereas reverse time migration has the great advantage of producing high-resolution images, it also requires a great deal of computational expenditure. Since modern computer technology provided the necessary computing power, reverse time migration is being actively studied.

For waveform inversion, the L_2-norm is generally used as an objective function. However, using the L_2-norm objective function may lead to distorted imaging because of its high sensitivity to outliers and non-Gaussian errors in field data (Clearbout and Muir, 1973). For this reason, many authors considered applying the L_1-norm objective function. To mitigate the sensitivity of the traditional waveform inversion to noise, Tarantola (1984) introduced the L_1-norm in time domain full waveform inversion, and Pyun et al. (2009) proposed using the L_1-norm in frequency domain waveform inversion. In addition, the Huber norm (Ha et al., 2009), sech criteria (Crase et al., 1990; Monteiller et al., 2005) and the hybrid L_1/L_2-norm were all considered to overcome the issue of noise sensitivity. These studies highlighted the robustness of the L_1-norm objective function in the waveform inversion algorithm with noisy data, particularly data outliers.

The reverse time migration algorithm is the same as the first iteration of the waveform inversion algorithm (Lailly, 1983; Tarantola, 1984). That is, reverse time migration has the same algorithm structure as waveform inversion (Shin et al., 2003; Chavent and Plessix, 1999). Reverse time migration back-propagates field data for convolving with virtual sources while waveform inversion back-propagates the residual vectors between field and modeled data (Pratt et al., 1998). This finding and the findings of earlier studies encourage us to consider the effectiveness of using the L_1-norm in the reverse time migration algorithm. This scheme is worth examining because most field data contain problematic outliers.

In this study, we adopt the L_1-norm in the frequency domain reverse time migration algorithm. In the following sections, we describe the theory of reverse time migration in the frequency domain and how the L_1-norm can be applied. We also depict a scaling method for obtaining clearer migration images, and a method for the suppression of migration artifacts. Then, we demonstrate our algorithm on synthetic data drawn from the Marmousi model. Because the

purpose of this paper is to show robustness of our algorithm against outliers, to have a comparison, we add outliers on the seismogram and carry out the identical experiments. We then evaluate our algorithm on field data obtained from the Gulf of Mexico. All the results from our algorithm are compared with those from conventional algorithm. Through these experiments, we show the effectiveness of our algorithm, which is frequency domain reverse time migration using the L_1-norm.

REVERSE TIME MIGRATION USING THE L_1-NORM

Reverse time migration

Reverse time migration can be expressed as a zero-lag cross correlation between the partial derivative wavefield with respect to the earth parameter and the observed wavefield in the survey:

$$\psi_m = \int_0^{T_{max}} \sum_{s=1}^{N_{shot}} \{[\partial \mathbf{u}_s(t)/\partial p_m]^T \mathbf{d}_s(t)\} dt \quad , \tag{1}$$

$$\mathbf{u}_s = (u_{s,1}, u_{s,2}, \ldots, u_{s,N_r}) \quad , \tag{2}$$

$$\mathbf{d}_s = (d_{s,1}, d_{s,2}, \ldots, d_{s,N_r}) \quad , \tag{3}$$

where ψ_m is the reverse time migration for the m-th model parameter, s is the shot number, N_{shot} is the total number of shots, T_{max} is the maximum record length, p_m is the m-th model parameter, and $\mathbf{u}_s$ and $\mathbf{d}_s$ are the vectors of modeled and observed wavefield, respectively (Shin and Chung, 1999). In this study, bold lettering stands for a vector, and T represents transpose of the vector. Thus, $\partial \mathbf{u}_s/\partial p_m$ is the vector of the partial derivative wavefield related to the m-th parameter by the s-th shot, and it can be interpreted as the sensitivity of the change of surface wavefield caused by slight fluctuations at the m-th position (Shin et al., 2003). In other words, eq. (1) shows that reverse time migration at the m-th position can be depicted as the sensitivity of the measured wavefield to the parameter at the m-th position (Shin et al., 2001). If we consider all the values of reverse time migration in the given portion of subsurface, the image of that portion can be obtained (Shin and Chung, 1999). We can also obtain reverse time migration in the frequency domain by Fourier transform of eq. (1):

$$\psi_m = \int_0^{\omega_{max}} \sum_{s=1}^{N_{shot}} \mathrm{Re}\{[\partial \tilde{\mathbf{u}}_s(\omega)/\partial p_m]^T \tilde{\mathbf{d}}_s^*(\omega)\} d\omega \quad , \tag{4}$$

where ω is the angular frequency, and $\tilde{\mathbf{u}}_s$ and $\tilde{\mathbf{d}}_s$ are the vectors of the modeled and observed wavefield in the frequency domain, respectively. * indicates the complex value, and Re indicates the real part of the complex value.

As we see from eq. (4), we now have to obtain the partial derivative wavefield. Accordingly, we can start from the wave equation. The 2D acoustic wave equation can be expressed in matrix form using the finite element method:

$$\mathbf{M}\ddot{\mathbf{u}}_s + \mathbf{C}\mathbf{u}_s + \mathbf{K}\mathbf{u}_s = \mathbf{f} \quad , \tag{5}$$

where $\mathbf{M}$ is the mass matrix, $\mathbf{C}$ is the damping matrix, $\mathbf{K}$ is the stiffness matrix, and $\mathbf{f}$ is the source vector (Marfurt, 1984; Zienkiewicz and Taylor, 1991). We can also represent wave equation in the frequency domain by using the Fourier transform:

$$\mathbf{S}\tilde{\mathbf{u}}_s = \tilde{\mathbf{f}} \quad , \tag{6}$$

$$\mathbf{S} = \mathbf{K} + i\omega\mathbf{C} + \omega^2\mathbf{M} \quad . \tag{7}$$

Then, the vector of the partial derivative wavefield can be obtained from the derivative of eq. (6) with respect to the model parameter (Pratt et al., 1998):

$$\mathbf{S}(\partial\tilde{\mathbf{u}}_s/\partial p_m) + (\partial\mathbf{S}/\partial p_m)\tilde{\mathbf{u}}_s = 0 \quad , \tag{8}$$

$$\partial\tilde{\mathbf{u}}_s/\partial p_m = \mathbf{S}^{-1}\mathbf{f}_{vs} \quad , \tag{9}$$

$$\mathbf{f}_{vs} = -(\partial\mathbf{S}/\partial p_m)\tilde{\mathbf{u}}_s \quad . \tag{10}$$

By comparing eq. (9) with (6), we see that $\mathbf{f}_{vs}$ corresponds to the source vector of the forward modeling algorithm while $\partial\tilde{\mathbf{u}}_s/\partial p_m$ corresponds to $\tilde{\mathbf{u}}_s$ of the forward modeling algorithm. Thus, $\mathbf{f}_{vs}$ is called the virtual source vector by the s-th shot.

Then, we can substitute eq. (9) into eq. (4):

$$\psi_m = \int_0^{\omega_{max}} \sum_{s=1}^{N_{shot}} \mathrm{Re}\{[\mathbf{S}^{-1}(\omega)\mathbf{f}_{vs}(\omega)]^T\mathbf{d}_s^*(\omega)\}d\omega \quad , \tag{11}$$

$$\psi_m = \int_0^{\omega_{max}} \sum_{s=1}^{N_{shot}} \mathrm{Re}\{\mathbf{f}_{vs}^T(\omega)[\mathbf{S}^{-1}(\omega)]^T\mathbf{d}_s^*(\omega)\}d\omega \quad . \tag{12}$$

Since the complex impedance matrix, **S** is symmetric,

$$\mathbf{S} = \mathbf{S}^{T} \quad . \tag{13}$$

Thus, eq. (12) gives

$$\psi_m = \int_0^{\omega_{max}} \sum_{s=1}^{N_{shot}} \mathrm{Re}[\mathbf{f}_{vs}^{T}(\omega)\mathbf{S}^{-1}(\omega)\tilde{\mathbf{d}}_s^{*}(\omega)]d\omega \quad . \tag{14}$$

Therefore, the m-th reverse time migration can be obtained by convolution of the back-propagated observed wavefield and virtual source, which can be established from a forward modeling algorithm. Moreover, we can obtain all the vectors of virtual sources in the given area of investigation when we consider all the parameters in that area. Ultimately, we can then obtain the complete set of values for reverse time migration in the given area.

Application of the L_1-norm objective function

First, we contrast the objective function of the L_1-norm with that of the L_2-norm in the waveform inversion algorithm to explain our algorithm more clearly. In the waveform inversion, we iteratively reduce the deviation between the forward modeled wavefield and the measured wavefield. Through this process, we iteratively reduce the deviation between the model parameter and the earth parameter. Thus, we can ultimately establish the earth parameter. In conventional waveform inversion, the L_2-norm is adopted to define the size of the residual between the modeled wavefield and the measured wavefield and is assigned as an objective function:

$$E = \tfrac{1}{2} \int_0^{\omega_{max}} \sum_{s=1}^{N_{shot}} [\tilde{\mathbf{u}}_s(\omega) - \tilde{\mathbf{d}}_s(\omega)]^{T}[\tilde{\mathbf{u}}_s(\omega) - \tilde{\mathbf{d}}_s(\omega)]^{*}d\omega \quad . \tag{15}$$

Through the minimization of this objective function, model parameters would approach the earth parameters. To minimize the objective function, we partially differentiate eq. (15) with respect to the model parameter:

$$\partial E/\partial p_m = \int_0^{\omega_{max}} \sum_{s=1}^{N_{shot}} \mathrm{Re}\{[\partial\tilde{\mathbf{u}}_s(\omega)/\partial p_m]^{T}[\tilde{\mathbf{u}}_s(\omega) - \tilde{\mathbf{d}}_s(\omega)]^{*}\}d\omega \quad . \tag{16}$$

We see that eqs. (16) and (4) have the same structure and compare them in Table 1. The gradient in the waveform inversion corresponds to reverse time migration. Moreover, the residual in waveform inversion corresponds to the observed wavefield in reverse time migration.

Table 1. Comparison between the gradient in waveform inversion and reverse time migration.

The gradient in waveform inversion	$\frac{\partial E}{\partial p_m} = \int_0^{\omega_{\max}} \sum_{s=1}^{N_{shot}} \mathrm{Re}\left\{ \left(\frac{\partial \tilde{\mathbf{u}}_s(\omega)}{\partial p_m} \right)^T \left(\tilde{\mathbf{u}}_s(\omega) - \tilde{\mathbf{d}}_s(\omega) \right)^* \right\} d\omega$
Reverse time migration	$\psi_m = \int_0^{\omega_{\max}} \sum_{s=1}^{N_{shot}} \mathrm{Re}\left\{ \left\{ \frac{\partial \tilde{\mathbf{u}}_s(\omega)}{\partial p_m} \right\}^T \tilde{\mathbf{d}}_s^*(\omega) \right\} d\omega$

Pyun et al. (2009), however, used the L_1-norm objective function to mitigate the effect of outliers:

$$E = \frac{1}{2} \int_0^{\omega_{\max}} \sum_{s=1}^{N_{shot}} \{ |\mathrm{Re}[\tilde{\mathbf{u}}_s(\omega) - \tilde{\mathbf{d}}_s(\omega)]| + |\mathrm{Im}[\tilde{\mathbf{u}}_s(\omega) - \tilde{\mathbf{d}}_s(\omega)]| \} d\omega \quad , \tag{17}$$

where Im is the imaginary part of the complex value. We also compare both objective functions in Table 2. To minimize this objective function, we also need a gradient:

$$\partial E / \partial p_m = \int_0^{\omega_{\max}} \sum_{s=1}^{N_{shot}} \mathrm{Re}\{ [\partial \tilde{\mathbf{u}}_s(\omega) / \partial p_m]^T \tilde{\mathbf{r}}_s^*(\omega) \} d\omega \quad , \tag{18}$$

$$\tilde{\mathbf{r}}_s = \mathrm{sgn}\{\mathrm{Re}[\tilde{\mathbf{u}}_s(\omega) - \tilde{\mathbf{d}}_s(\omega)]\} + i\,\mathrm{sgn}\{\mathrm{Im}[\tilde{\mathbf{u}}_s(\omega) - \tilde{\mathbf{d}}_s(\omega)]\} \quad , \tag{19}$$

Table 2. Comparison between the L_2-norm objective function and the L_1-norm objective function.

L_2-norm objective function	$E = \frac{1}{2} \int_0^{\omega_{\max}} \sum_{s=1}^{N_{shot}} \left[\tilde{\mathbf{u}}_s(\omega) - \tilde{\mathbf{d}}_s(\omega) \right]^T \left[\tilde{\mathbf{u}}_s(\omega) - \tilde{\mathbf{d}}_s(\omega) \right]^* d\omega$
L_1-norm objective function	$E = \frac{1}{2} \int_0^{\omega_{\max}} \sum_{s=1}^{N_{shot}} \left\{ \left| \mathrm{Re}\left[\tilde{\mathbf{u}}_s(\omega) - \tilde{\mathbf{d}}_s(\omega) \right] \right| + \left| \mathrm{Im}\left[\tilde{\mathbf{u}}_s(\omega) - \tilde{\mathbf{d}}_s(\omega) \right] \right| \right\} d\omega$

where sgn is the signum function. In Table 3, we compare the gradient of the L_2-norm objective function and that of the L_1-norm objective function.

Table 3. Comparison between the gradient of the L_2-norm objective function and the gradient of the L_1-norm objective function.

The gradient of L_2-norm objective function	$\frac{\partial E}{\partial p_m} = \int_0^{\omega_{\max}} \sum_{s=1}^{N_{shot}} \mathrm{Re}\left\{ \left(\frac{\partial \tilde{\mathbf{u}}_s(\omega)}{\partial p_m} \right)^T \left(\tilde{\mathbf{u}}_s(\omega) - \tilde{\mathbf{d}}_s(\omega) \right)^* \right\} d\omega$
The gradient of L_1-norm objective function	$\frac{\partial E}{\partial p_m} = \int_0^{\omega_{\max}} \sum_{s=1}^{N_{shot}} \mathrm{Re}\left\{ \left(\frac{\partial \tilde{\mathbf{u}}_s(\omega)}{\partial p_m} \right)^T \tilde{\mathbf{r}}_s^*(\omega) \right\} d\omega$ $\tilde{\mathbf{r}}_s = \mathrm{sgn}\left(\mathrm{Re}\left[\tilde{\mathbf{u}}_s(\omega) - \tilde{\mathbf{d}}_s(\omega) \right] \right) + i\,\mathrm{sgn}\left(\mathrm{Im}\left[\tilde{\mathbf{u}}_s(\omega) - \tilde{\mathbf{d}}_s(\omega) \right] \right)$

Hence, we adopt the L_1-norm in reverse time migration algorithm in the frequency domain:

$$\psi_m = \int_0^{\omega_{\max}} \sum_{s=1}^{N_{shot}} \mathrm{Re}\{[\partial \tilde{\mathbf{u}}_s(\omega)/\partial p_m]^T \tilde{\mathbf{x}}_s^*(\omega)\} d\omega \quad , \tag{20}$$

$$\tilde{\mathbf{x}}_s = \mathrm{sgn}\{\mathrm{Re}[\tilde{\mathbf{d}}_s(\omega)]\} + i\,\mathrm{sgn}\{\mathrm{Im}[\tilde{\mathbf{d}}_s(\omega)]\} \quad . \tag{21}$$

Table 4. Comparison between the gradient in waveform inversion and reverse time migration when using the L_1-norm.

The gradient in waveform inversion using L_1-norm	$\frac{\partial E}{\partial p_m} = \int_0^{\omega_{\max}} \sum_{s=1}^{N_{shot}} \mathrm{Re}\left\{ \left(\frac{\partial \tilde{\mathbf{u}}_s(\omega)}{\partial p_m} \right)^T \tilde{\mathbf{r}}_s^*(\omega) \right\} d\omega$ $\tilde{\mathbf{r}}_s = \mathrm{sgn}\left(\mathrm{Re}\left[\tilde{\mathbf{u}}_s(\omega) - \tilde{\mathbf{d}}_s(\omega) \right] \right) + i\,\mathrm{sgn}\left(\mathrm{Im}\left[\tilde{\mathbf{u}}_s(\omega) - \tilde{\mathbf{d}}_s(\omega) \right] \right)$
Reverse time migration using L_1-norm	$\psi_m = \int_0^{\omega_{\max}} \sum_{s=1}^{N_{shot}} \mathrm{Re}\left\{ \left[\frac{\partial \tilde{\mathbf{u}}_s(\omega)}{\partial p_m} \right]^T \tilde{\mathbf{x}}_s^*(\omega) \right\} d\omega$ $\tilde{\mathbf{x}}_s = \mathrm{sgn}\left(\mathrm{Re}\left[\tilde{\mathbf{d}}_s(\omega) \right] \right) + i\,\mathrm{sgn}\left(\mathrm{Im}\left[\tilde{\mathbf{d}}_s(\omega) \right] \right)$

In other words, we can obtain the reverse time migration algorithm using the L_1-norm by replacing the vector of the residual in the waveform inversion using the L_1-norm with the vector of measured wavefield.

We can obtain reverse time migration by exploiting the vector of the observed wavefield instead of the vector of residual in the waveform inversion using the L_1-norm, as we conventionally use the L_2-norm. In Table 4, we compare waveform inversion and the reverse time migration algorithm which use the L_1-norm. Finally, in Table 5, we compare conventional reverse time migration using the L_2-norm and newly proposed reverse time migration using the L_1-norm. In the 'Numerical Example' section below, we compare the results of these two algorithms to verify the effectiveness of our algorithm.

Table 5. Comparison between the conventional algorithm using the L_2-norm and our algorithm using the L_1-norm.

Conventional algorithm	$\psi_m = \int_0^{\omega_{\max}} \sum_{s=1}^{N_{shot}} \mathrm{Re}\left\{ \left\{ \frac{\partial \tilde{\mathbf{u}}_s(\omega)}{\partial p_m} \right\}^T \tilde{\mathbf{d}}_s^*(\omega) \right\} d\omega$
Our algorithm	$\psi_m = \int_0^{\omega_{\max}} \sum_{s=1}^{N_{shot}} \mathrm{Re}\left\{ \left[\frac{\partial \tilde{\mathbf{u}}_s(\omega)}{\partial p_m} \right]^T \tilde{\mathbf{x}}_s^*(\omega) \right\} d\omega$ $\tilde{\mathbf{x}}_s = \mathrm{sgn}\left(\mathrm{Re}\left[\tilde{\mathbf{d}}_s(\omega)\right]\right) + i\,\mathrm{sgn}\left(\mathrm{Im}\left[\tilde{\mathbf{d}}_s(\omega)\right]\right)$

Scaling method

When we consider all the given elements, eq. (18) can be rewritten as:

$$\psi = \int_0^{\omega_{\max}} \sum_{s=1}^{N_{shot}} \mathbf{J}_s^T(\omega)\tilde{\mathbf{x}}_s^*(\omega)\mathrm{d}\omega \quad , \tag{22}$$

If we use this equation as written, the seismic image at later times can be faint because of geometrical spreading. We can enhance the image and mitigate this effect by dividing by a Hessian matrix. Pratt et al. (1998) proposed applying the Gauss-Newton method to the waveform inversion:

$$\int_0^{\omega_{max}} \sum_{s=1}^{N_{shot}} \mathbf{J}_s^T(\omega)\mathbf{J}_s(\omega)d\omega\,\mathbf{p} = \psi \quad , \tag{23}$$

where $\mathbf{J}_s^T\mathbf{J}_s$ refers to the approximate Hessian matrix (Dennis, 1997). The components of the main diagonal of the approximate Hessian matrix are the zero-lag autocorrelations of the partial-derivative wavefields, which are always positive. Numerical correlations of wavefields' on the off-diagonal, on the other hand, are far smaller than those on the main diagonal and are negligible quantities. Thus, we can use only the components on the main diagonal for the scaling:

$$\mathbf{p} \simeq \{\psi \,/\, \int_0^{\omega_{max}} \sum_{s=1}^{N_{shot}} \mathrm{diag}[\mathbf{J}_s^T(\omega)\mathbf{J}_s(\omega)]d\omega\}$$

$$= \int_0^{\omega_{max}} \sum_{s=1}^{N_{shot}} \mathbf{J}_s^T(\omega)\tilde{\mathbf{x}}_s^*(\omega)d\omega \,/\, \int_0^{\omega_{max}} \sum_{s=1}^{N_{shot}} \mathrm{diag}[\mathbf{J}_s^T(\omega)\mathbf{J}_s(\omega)]d\omega \quad . \tag{24}$$

However, eq. (24) is difficult to compute when the Jacobian matrix is large. Shin et al. (2001) proposed pseudo-Hessian matrix, $\mathbf{F}_{vs}^{*T}\mathbf{F}_{vs}$, as an alternative. The virtual source matrix of the s-th shot is expressed in $\mathbf{F}_{vs}$, which considers the virtual source vector of the s-th shot, $\mathbf{f}_{vs}$ at every element. Off-diagonal components of the virtual matrix are also negligible:

$$\mathbf{p} \simeq \int_0^{\omega_{max}} \sum_{s=1}^{N_{shot}} \mathbf{J}_s^T(\omega)\tilde{\mathbf{x}}_s^*(\omega)d\omega \,/\, \int_0^{\omega_{max}} \sum_{s=1}^{N_{shot}} \mathrm{diag}[\mathbf{F}_{vs}^{*T}(\omega)\mathbf{F}_{vs}(\omega)]d\omega \quad , \tag{25}$$

In addition, we do not need to compute the Jacobian matrix if we use back-propagation:

$$\mathbf{p} \simeq \int_0^{\omega_{max}} \sum_{s=1}^{N_{shot}} \mathbf{F}_{vs}^T(\omega)\mathbf{S}^{-1}(\omega)\tilde{\mathbf{x}}_s^*(\omega)d\omega \,/\, \int_0^{\omega_{max}} \sum_{s=1}^{N_{shot}} \mathrm{diag}[\mathbf{F}_{vs}^{*T}(\omega)\mathbf{F}_{vs}(\omega)]d\omega \quad . \tag{26}$$

In this study, we follow Shin et al.'s (2001) proposal and Jang et al.'s (2009) first scaling method, which minimize the effects of the band-limited source spectrum by normalizing every frequency:

$$\mathbf{p} \simeq \int_0^{\omega_{max}} \mathrm{NRM}[\sum_{s=1}^{N_{shot}} \mathrm{Re}[\mathbf{F}_{vs}^T(\omega)\mathbf{S}^{-1}(\omega)\tilde{\mathbf{x}}_s^*(\omega)]$$

$$/ \sum_{s=1}^{N_{shot}} \mathrm{Re}\{\mathrm{diag}[\mathbf{F}_{vs}^{*T}(\omega)\mathbf{F}_{vs}(\omega) + \lambda\mathbf{I}]\}]d\omega \quad , \tag{27}$$

where NRM stands for the normalization, λ is the damping factor, and **I** is the identity matrix.

The suppression of artifacts

Diving waves, head waves, backscattered waves, and so on can be cross-correlated in the process of migration, thus producing artifacts. To suppress these artifacts, we use a vertical derivative filter. Filtering the final image may compromise the integrity of the signal of interest, but it is convenient to use and can produce good results (Guitton et al., 2007). After we apply both first-order and second-order derivative filters, we select the better result from the two.

NUMERICAL EXAMPLES

Marmousi model

To verify the effectiveness of our algorithm using the L_1-norm, we demonstrate it using the Marmousi model (Fig. 1a). We carry out both the conventional and proposed reverse time migration and compare the results. We synthesize seismograms through 2D acoustic frequency-domain forward modeling with the finite element method. To express the wave equation in matrix form, we use an eclectic mass matrix and stiffness matrix, as proposed by Marfurt (1984). The grid interval is 4 m, shot interval is 24 m, and receiver interval is 4 m. All the shots and receivers are assumed to be located 4 m below the free surface. We assume all the shots and receivers to be present on all grid nodes except along the boundary to apply boundary condition. Thus, we use 384 shots, with 2301 receivers for each shot, the Dirichlet boundary condition (Officer, 1958) along the free surface, and an absorbing boundary condition (Clayton and Enquist, 1977) along both sides and the base. The maximum record length and sampling interval are 5 s and 0.0125 s, respectively. The frequency ranges from 0.2 to 40 Hz, and the frequency interval is 0.2 Hz.

Fig. 2a is the common shot gather with a shot located at the center of the surface layer. Then, we artificially add some random outliers on the seismogram to investigate the robustness of our algorithm in the presence outliers. Fig. 2b shows the common shot gather including outliers when a shot is located at the center of the surface. We perform conventional and proposed reverse time migration on both the seismogram without outliers and the seismogram containing outliers. The background model used is the smoothed Marmousi model shown in Fig. 1b. As we stated in the preceding section, we use a pseudo Hessian matrix for the scaling and a first-order derivative filter for the suppression of artifacts.

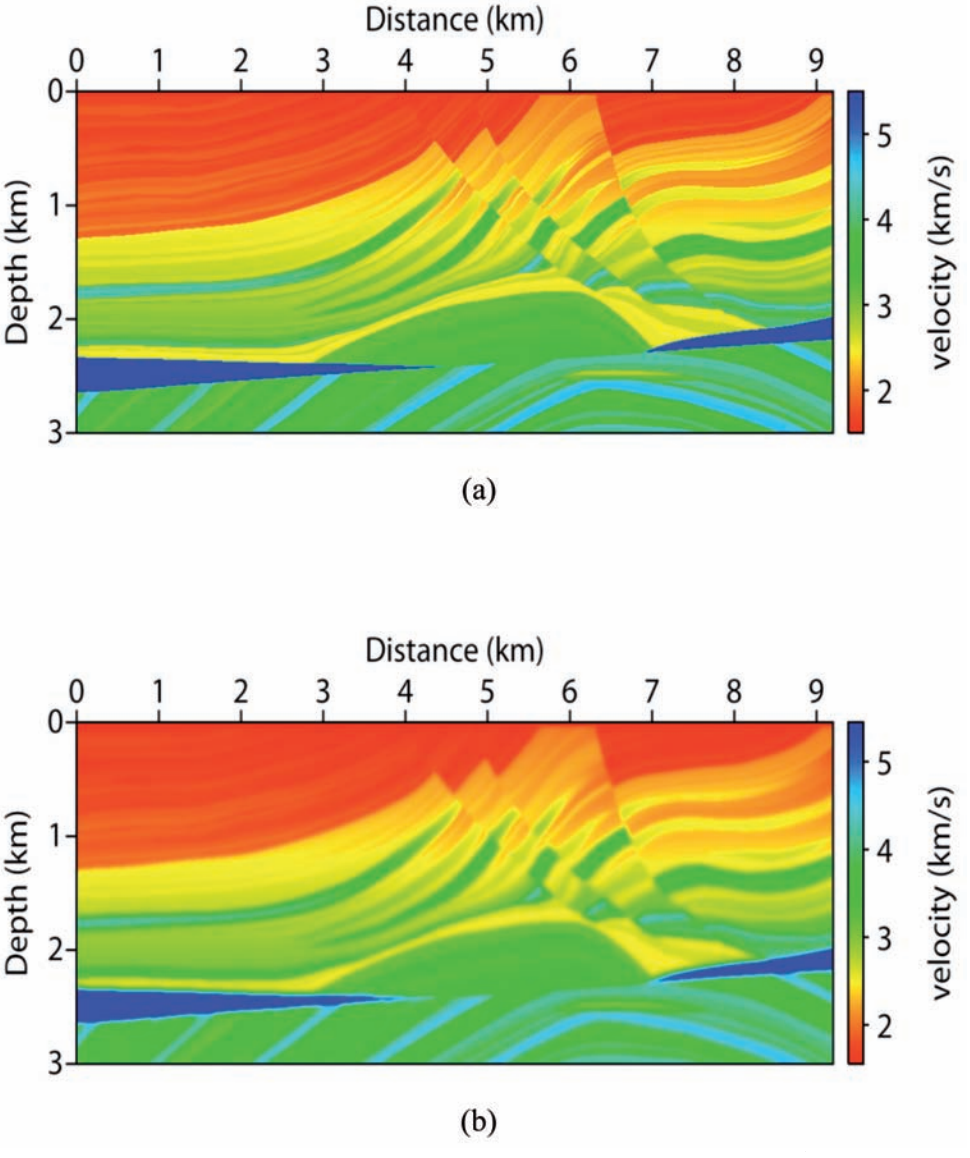

Fig. 1. (a) The Marmousi model and (b) a smoothed version of it.

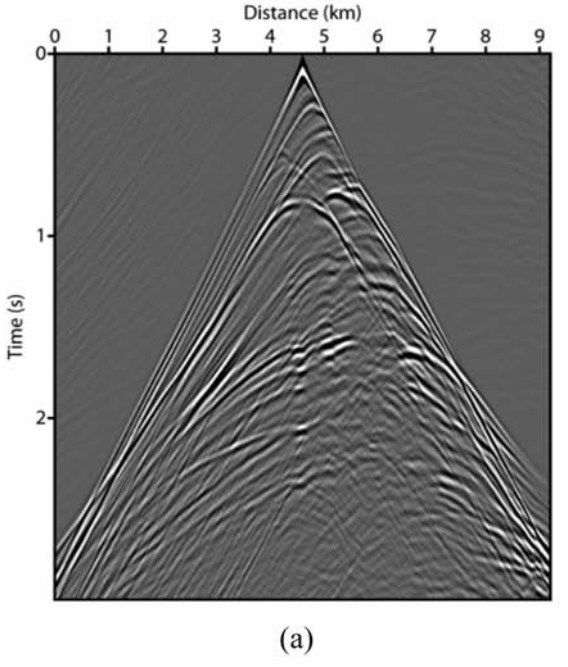

(a)

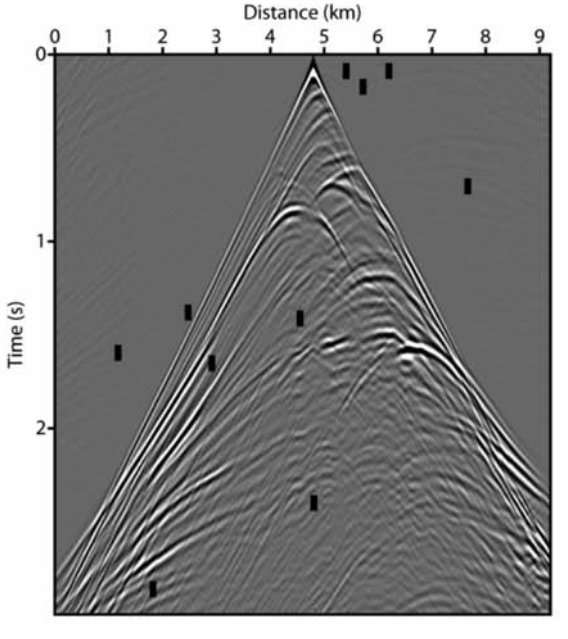

(b)

Fig. 2. (a) A synthesized common shot gather from the Marmousi model and (b) added outliers to the shot gather.

Through these numerical experiments, we see the results that we expected. First, we apply the conventional algorithm and our new algorithm to the seismogram without outliers and find that both algorithms produce similar results. Fig. 3a shows the migrated image obtained through the conventional algorithm using the L_2-norm whereas Fig. 3b shows the migrated image obtained through our new algorithm using the L_1-norm. We observe that these results are almost the same. However, the results do appear to be different when we apply the conventional algorithm and the new algorithm to seismograms to which we added artificial outliers. The new algorithm using the L_1-norm yields far better results. Fig. 4a shows the migrated image obtained through the conventional algorithm using the L_2-norm. In this result, we can see wedge shaped noise at the surface layer. Moreover, structures near the surface and on both sides are blurred. Fig. 4b shows the migrated image obtained through our new algorithm using the L_1-norm. This algorithm does not generate any noise near the surface layer. Furthermore, we see that all the structures resulting from our algorithm are clearer and more focused than those of the conventional algorithm; indeed, Figs. 3b and 4b are almost the same without reference to the existence of outliers. We speculate that the effect of outliers is reduced because measured wavefields are judged only by the signs of their real and imaginary components when using the L_1-norm. We also suspect that these results indicate the robustness of our algorithm when using the L_1-norm on synthetic data.

Field data

To examine the feasibility of using our algorithm on real seismic data, we apply our algorithm to a dataset recorded in the Gulf of Mexico. Fig. 5 is the 100-th common shot gather from this dataset. Noise and null traces are easily observed. The data consist of 399 shots with 407 receivers for each shot. The shot interval and receiver interval are 50 m and 25 m, respectively. The minimum and maximum offsets are 137 m and 10,292 m, respectively. The maximum record length is 12 s, the sampling interval is 4 ms, the frequency interval is 0.03052 Hz, and the frequency ranges from 0.0352 to 36 Hz. We cannot define a source wavelet from these field data; hence, we use source estimation to obtain source wavelet. We used a pseudo Hessian matrix and second-order derivative to improve the results.

As we expected, our algorithm using the L_1-norm yields better results than prior methods. Fig. 6a shows the reverse time migration when using a conventional algorithm using the L_2-norm. In this result, distinct erratic artifacts on both sides of a salt body distract from interpretation of the original structure. Fig. 6b is the reverse time migration using our algorithm with the L_1-norm. We see fainter erratic artifacts in Fig. 6b, especially in the circled areas in each migration section. We also notice that artifacts in the salt body, marked with

arrows, are fainter in Fig. 6b than in Fig. 6a. And the reflectors at the top of the salt body are more markedly distinguishable from artifacts in Fig. 6b. Especially in the area to the right, marked with an arrow, we see a clear distinction between Figs. 6a and 6b. Moreover, continuity of reflectors is also

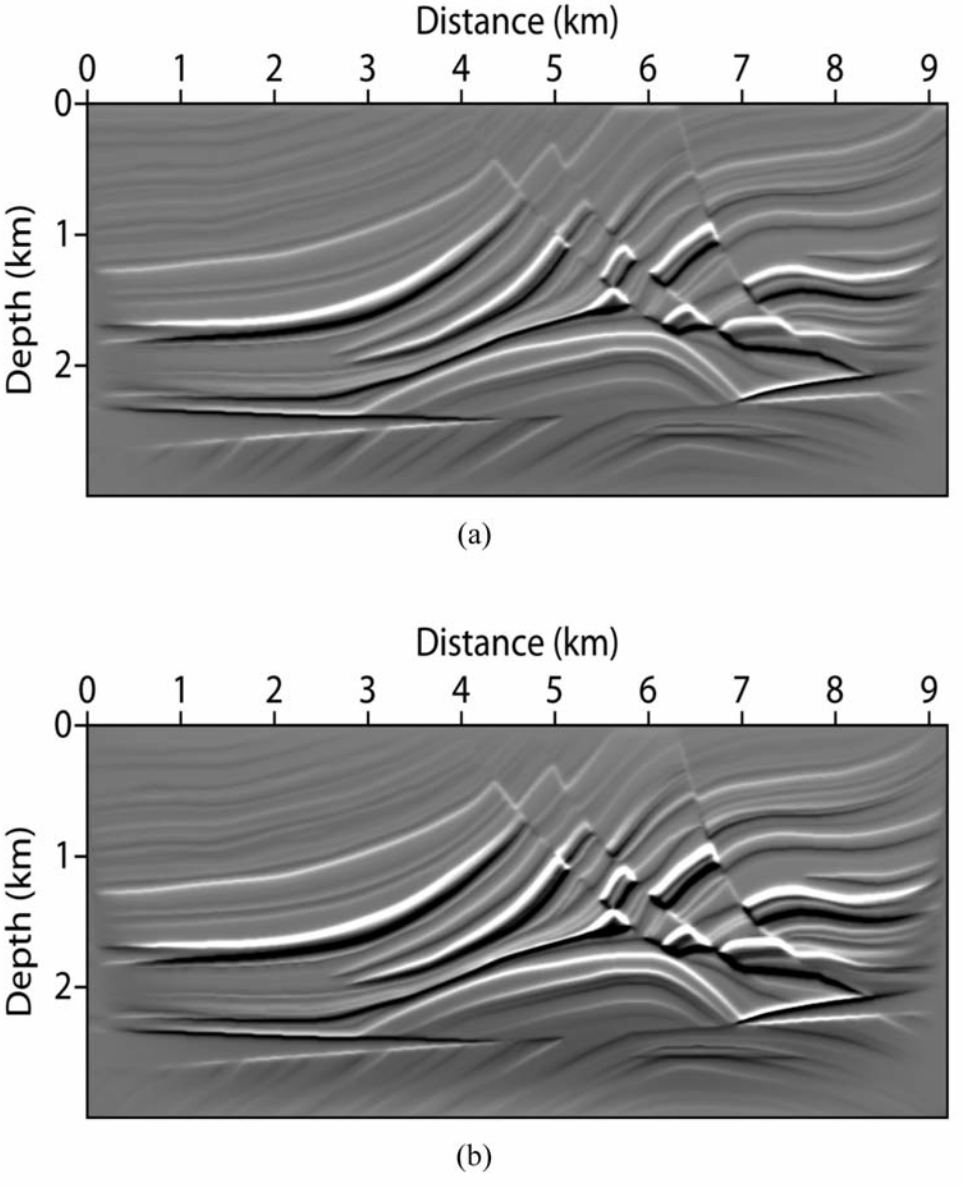

Fig. 3. Migrated image of the data without outliers using (a) the conventional algorithm and (b) the new algorithm.

better expressed in Fig. 6b than in Fig. 6a. We mark it off with arrows and display their close-up in the Figs. 7a and 7b, respectively. We propose that these results indicate the effectiveness of our algorithm using the L_1-norm for real seismic data, as well as synthetic data.

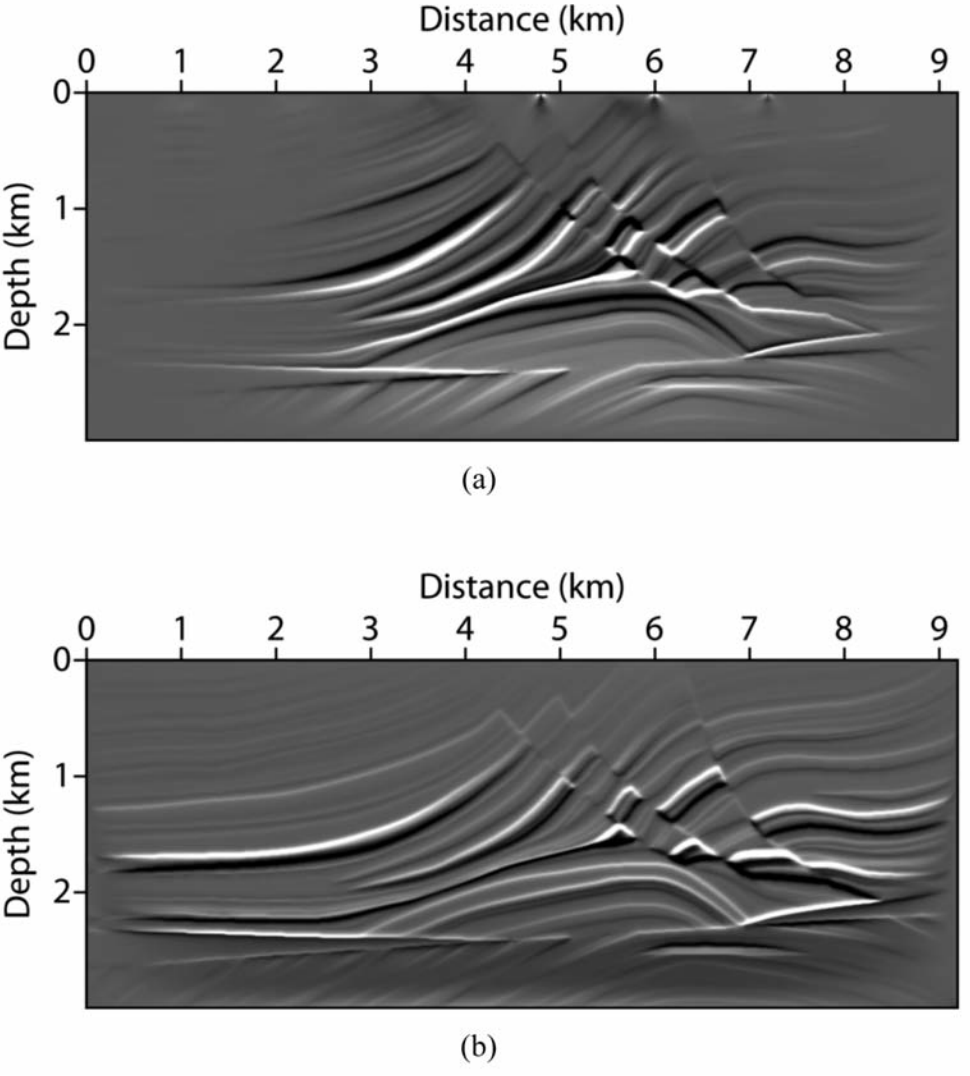

Fig. 4. Migrated image of the data containing outliers using (a) the conventional algorithm and (b) the new algorithm.

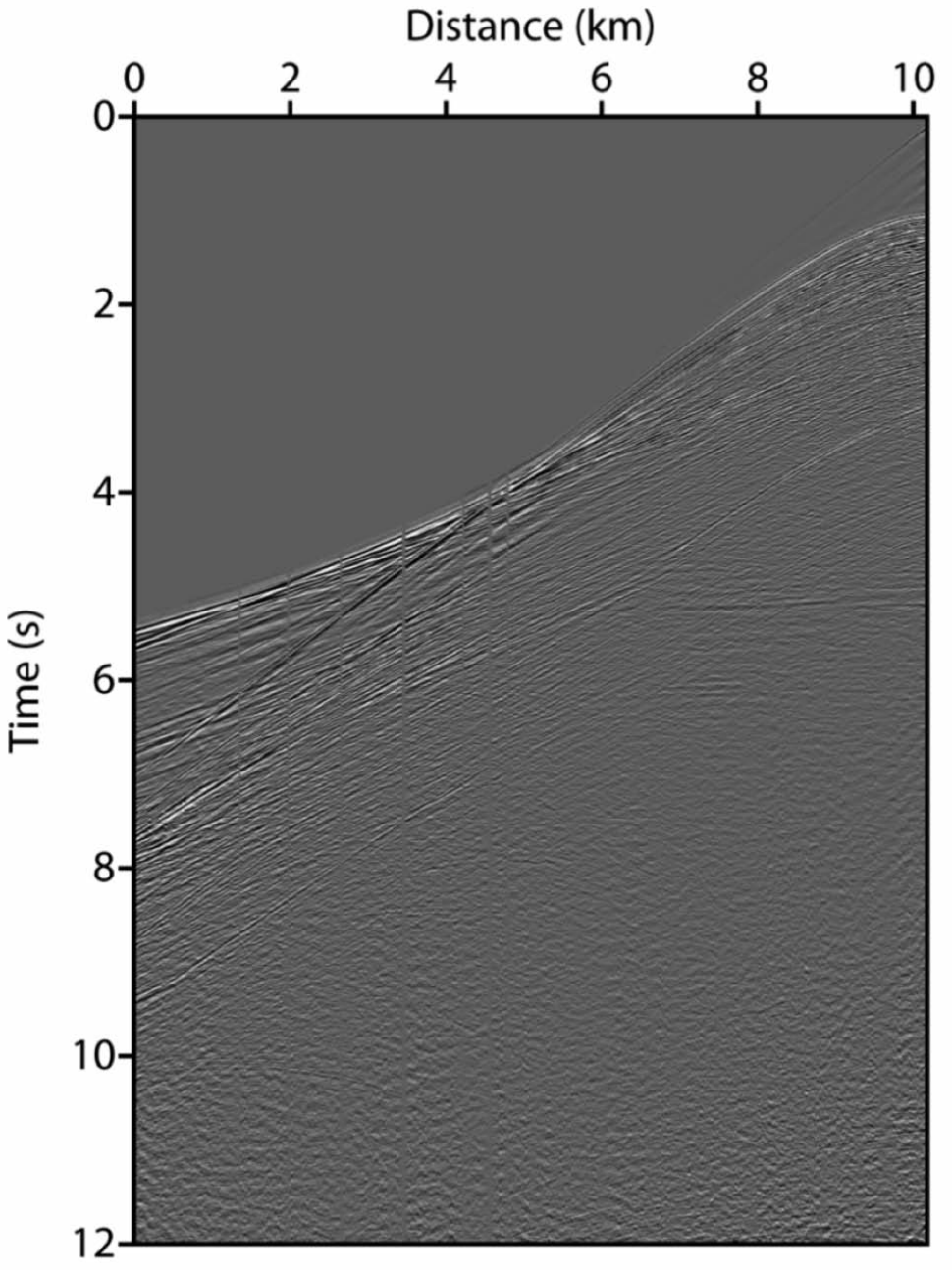

Fig. 5. The Common shot gather taken from the Gulf of Mexico dataset.

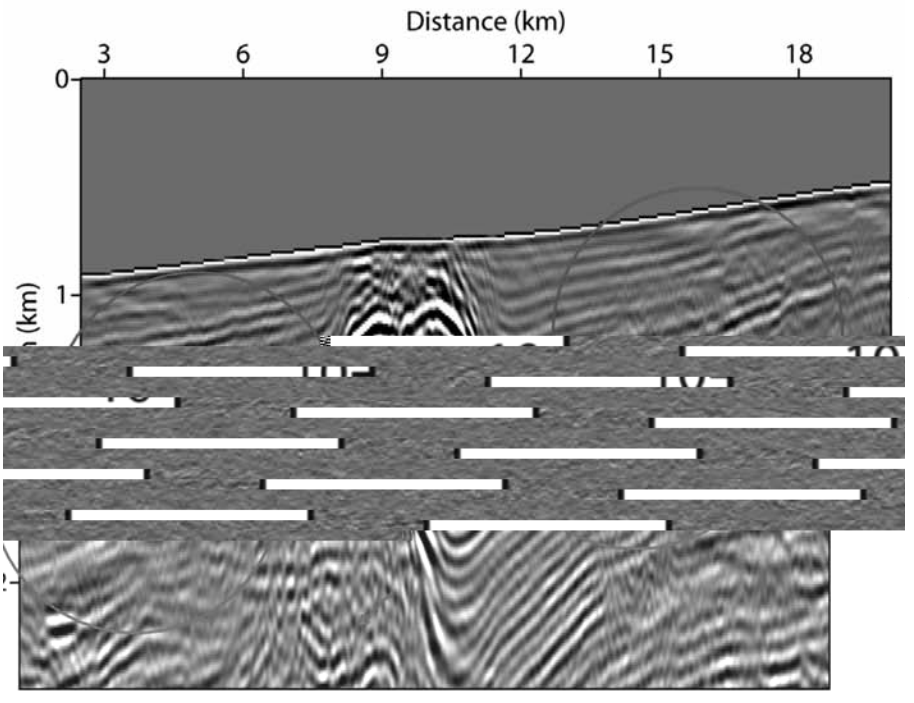

(a)

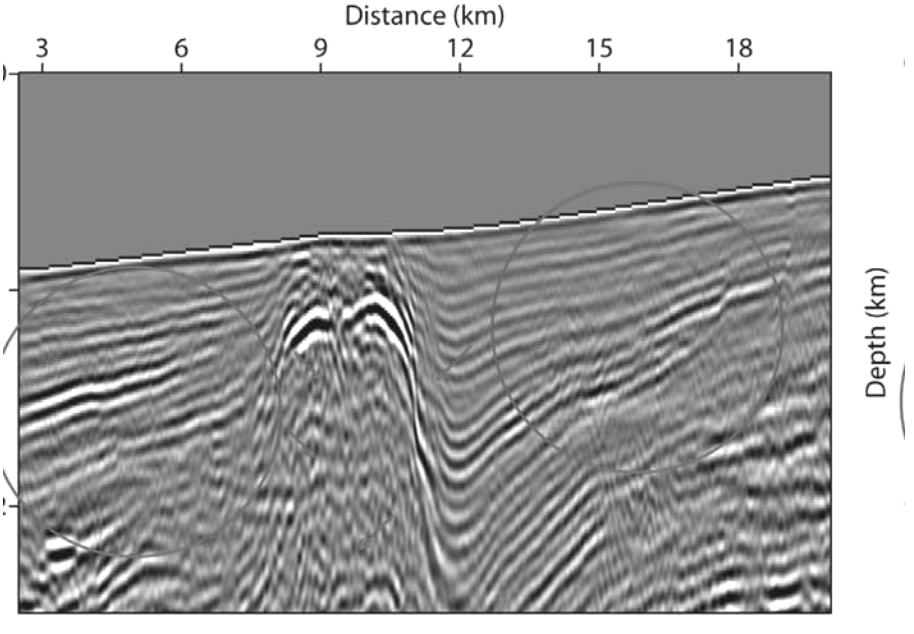

Fig. 6. Migrated image obtained by (a) a conventional algorithm and (b) the new algorithm.

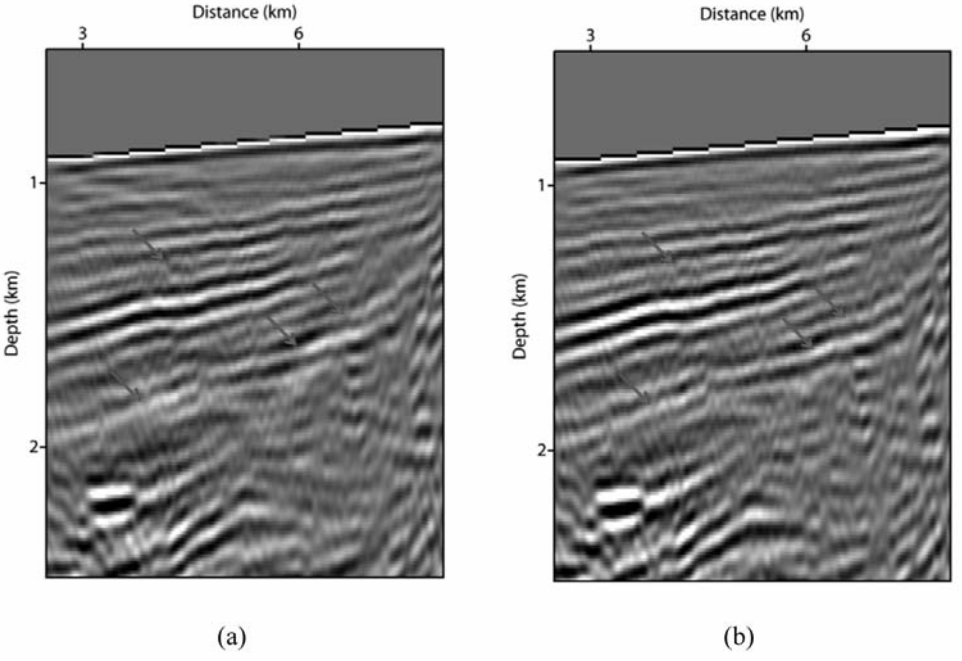

Fig. 7. Close-up of migrated image obtained by (a) a conventional algorithm and (b) the new algorithm.

CONCLUSION

Since the L_2-norm may produce a distorted image because of the sensitivity to outliers, some studies proposed waveform inversion using the L_1-norm. Consequently, we propose to adopt the L_1-norm in the reverse time migration algorithm. We hypothesized that the L_1-norm could reduce the effect of outliers because measured data are judged by only the sings of their real and imaginary components in our algorithm.

Through our numerical experiments, we confirm the robustness of the new algorithm. With synthetic data, from the Marmousi model, our algorithm yields better results than conventional algorithms on data that contains outliers, while both algorithms yield similar results on data without outliers. With regard to field data, as expected from the synthetic results, our algorithm yields better results. We conclude, therefore, that the new algorithm using the -norm for reverse time migration can be useful for field data containing considerable outliers. Furthermore, we expect that our algorithm can reduce, somewhat, the need for pre-processing efforts.

ACKNOWLEDGEMENT

This work was supported by the Energy Efficiency & Resources of the Korea Institute of Energy Technology Evaluation and Planning (KETEP) grant funded by Korea government Ministry of Knowledge Economy (No.2010T100200376).

REFERENCES

Baysal, E., Kosloff, D.D. and Sherwood, J.W.C., 1983. Reverse time migration. Geophysics, 48: 1514-1524.

Chavent, G. and Plessix, R.E., 1999. An optimal true-amplitude least-squares prestack depth-migration operator. Geophysics, 64: 508-515.

Claerbout, J.F. and Muir, F., 1973. Robust modeling with erratic data. Geophysics, 38: 826-844.

Clayton, R. and Enquist, B., 1977. Absorbing boundary conditions for acoustic and elastic wave equations. Bull. Seismol. Soc. Am., 67: 1529-1540.

Crase, E., Pica, A., Noble, M., McDonald, J. and Tarantola, A., 1990. Robust elastic nonlinear waveform inversion; application to real data. Geophysics, 55: 527-538.

Dennis, J., 1997. Nonlinear least squares and equations. In: Jacobs, D. (Ed.), The State of the Art of Numerical Analysis. Academic Press, Inc., New York.

Guitton, A., Kaelin, B. and Biondi, B., 2007. Least-squares attenuation of reverse-time-migration artifacts. Geophysics, 72: 19-23.

Ha, T., Chung, W. and Shin, C., 2009. Waveform inversion using a back-propagation algorithm and a Huber function norm. Geophysics, 74: 15-24.

Jang, U., Min, D.-J. and Shin, C., 2009. Comparison of scaling methods for waveform inversion. Geophys. Prosp., 57: 49-59.

Lailly, P., 1983. The seismic inverse problem as a sequence of before stack migrations. Conf. on Inverse Scattering, Theory and Applied Mathematics, Expanded Abstr.: 206-220.

Loewenthal, D. and Mufti, I.R., 1983. Reverse time migration in spatial frequency domain. Geophysics, 48: 627-635.

Marfurt, K.J., 1984. Accuracy of finite-difference and finite-element modeling of the scalar and elastic wave equation. Geophysics, 49: 533-549.

Monteiller, V., Got, J.-L., Virieux, J. and Okubo, P.G., 2005. An efficient algorithm for double-difference tomography and location in heterogeneous media, with an application to the Kilauea volcano. J. Geophys. Res., 110: B12306, doi:10.1029/2004JB003466

Officer, C.B., 1958. Introduction to the Theory of Sound Transmission with Application to the Ocean. McGraw-Hill, New York.

Pratt, R.G., Shin, C. and Hicks, G.J., 1998. Gauss-Newton and full Newton methods in frequency-space seismic waveform inversion. Geophys. J. Internat., 133: 341-362.

Pyun, S., Son, W. and Shin, C., 2009. Frequency-domain waveform inversion using an -norm objective function. Explor. Geophys., 40: 227-232.

Shin, C. and Chung, S., 1999. Understanding CMP stacking hyperbola in terms of partial derivative wavefield. Geophysics, 64: 1774-1782.

Shin, C., Jang, S. and Min, D.-J., 2001. Improved amplitude preservation for prestack depth migration by inverse scattering theory. Geophys. Prosp., 49: 592-606.

Shin, C., Min, D.-J., Yang, D. and Lee, S.K., 2003. Evaluation of poststack migration in terms of virtual source and partial derivative wavefields. J. Seismic Explor., 12: 17-37.

Tarantola, A., 1984. Inversion of seismic reflection data in the acoustic approximation. Geophysics, 49: 1259-1266.

Whitmore, N.D., 1983. Iterative depth migration by backward time propagation. Expanded Abstr., 53rd Ann. Internat. SEG Mtg., Las Vegas.

Zienkiewicz, O.C. and Taylor, R.L., 1991. The Finite Element Method, 4th ed. McGraw Hill Higher Education, New York.